Electronic and magnetic properties of zigzag graphene nanoribbons with periodic protruded edges

Wenzhi Wu, Zhuhua Zhang, Peng Lu, and Wanlin Guo*
Institute of Nanoscience, Nanjing University of Aeronautics and Astronautics, Nanjing 210016, China
(Received 22 March 2010; published 17 August 2010)

The electronic and magnetic properties of zigzag graphene nanoribbons with protruded steps along their edges (ZS-GNRs) are investigated by extensive density-functional theory calculations. We show that the electronic and magnetic properties are determined by an interesting interplay between the length of the protruded step and the distance of two adjacent steps along the ribbon edge. With a small length of the protruded steps along the edge, the system can be converted from a nonmagnetic semiconductor to metal and then to a magnetic semiconductor by increasing the step-to-step distance. In particular, the energy gap decreases first toward a zero minimum and then gradually increases as the step length increases, accompanying with the rapid increase in the edge magnetization. When the step length exceeds a critical value, the ZS-GNR will be always a magnetic semiconductor regardless of the step-to-step distance. We also reveal that the applied transverse electric field can enlarge the energy gap of nonmagnetic ZS-GNRs, due to the breaking of band degeneration; whereas the field-induced gap change in the magnetic ZS-GNRs is spin dependent, leading to the emergence of amazing half metallicity under certain field strengths. These findings suggest that the ZS-GNRs are promising for designing versatile graphene-based devices and can find novel applications in both electronics and spintronics.

DOI: 10.1103/PhysRevB.82.085425 PACS number(s): 73.22.Pr, 73.20.At, 75.75.−c, 71.15.Mb

I. INTRODUCTION

Graphene, a single graphite layer, is emerging as an extremely versatile material with outstanding properties[1–11] for spintronics and nanodevice applications.[11–13] Nevertheless, graphene is a zero band-gap semiconductor and is unable to electrostatically confine electrons for development of graphene-based field-effect transistors. An important approach for opening the band gap is to pattern the graphene sheet into narrow ribbons[2,14,15] with width less than 10 nm. Owing to the edge effect, the electronic wave functions in the direction perpendicular to the ribbon edge can be confined and quantized. Such confinement-induced quantization induces a band gap around the Fermi level.[16,17] Especially, the zigzag-edged graphene nanoribbons (Z-GNRs) are predicted to be magnetic semiconductor [antiferromagnetic (AFM)],[16] where the polarized electron spins are ferromagnetically aligned along the ribbon edges and antiferromagnetically coupled between the two edges. Such amazing spin ordering can give rise to many unusual properties such as giant magnetoresistance effect,[13] half metallic[17] and magnetoelectric effect,[18] and promising applications. However, all these theoretical studies mainly focus on the Z-GNRs with smooth edges. Actually, under typical growth or fabrication conditions, the edges of graphene ribbons are often observed to be rough and tapered by 5–10 Å steps protruded out of the edges. Also, recent experiments demonstrated that carbon nanotubes can be stepwisely opened along their tube axis by controlling the size of transition-metal nanoparticles, producing graphene nanoribbons with regular steplike edges.[19] This form of edge roughness would be significant in determining the GNRs properties considering that the spin-polarized edge states in Z-GNRs are easily affected by structural perturbation, such as defect,[20–25] the presence of substrate,[26] and chemical functionalizations.[27] On the other hand, shaping the graphene with diverse edge configuration also offers a promising opportunity to tailor its properties. Recent theoretical study showed that tapered silicon nanowires can show unique electronic and optical properties to their counterparts with smooth surfaces.[28] To our knowledge, however, how the edge steps affect the electronic and magnetic properties of the Z-GNRs remains completely elusive, although there are some empirical tight-binding studies addressed on this issue.

In this paper, we have investigated the structural and electronic properties of zigzag graphene nanoribbons with protruded steps along their edges (ZS-GNRs) by using state-of-the-art first-principles calculations. We show that the electronic and magnetic properties can be widely tuned by changing the step length as well as the distance of two adjacent steps along the ribbon edge. As a result, with a short step length, the ZS-GNRs can undergo an interesting evolution from nonmagnetic (NM) semiconductor to nonmagnetic metal and finally to magnetic semiconductor. Also, we show that applied external electric fields can strongly influence the electronic and magnetic properties of the system, and it can lead to important functions, such as metal-insulator transition and half metal, rendering the ZS-GNRs a versatile candidate for designing novel electronic and spintronic devices.

II. MODEL GEOMETRY AND CALCULATION METHODS

All the calculations are performed within the framework of density-functional theory (DFT) by using the plane-wave basis set with VASP code.[29] The ultrasoft pseudopotentials[30] are employed for the ionic potential and the local spin-density approximation (LSDA) is used to describe the exchange-correlation potential. We also performed test calculations using generalized gradient approximation (GGA) and the results are qualitatively the same. We use the supercell geometry where the ZS-GNR is separated by 10 Å in

 ©2010 The American Physical Society

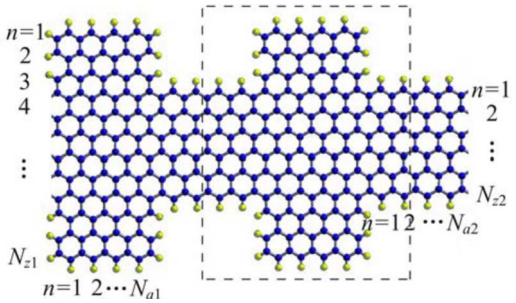

FIG. 1. (Color online) Atomic structures of ZS-GNR(N_{z1}, N_{a1}; N_{z2}, N_{a2}). The ZS-GNR consists of two parts: wider quasi-Z_{Nz1}-GNR and narrower quasi-Z_{Nz2}-GNR, which are alternatively aligned along the ribbon edge, where N_{zi} (i=1 and 2) is the number of zigzag chains across the ribbon width and N_{ai} (i=1 and 2) is measured by the number of hexagonal rings along the ribbon length. The blue and yellow balls represent the carbon and terminated hydrogen atoms, respectively. The dash rectangle represents the supercell of ZS-GNRs used in our calculations.

both normal and parallel directions to adjacent ribbons to simulate an isolated ZS-GNR. The conjugate gradient method is used to optimize the geometry and all the atoms in the unit cell are fully relaxed until the force on each atom is less than 0.01 eV/Å. The Brillouin-zone integration is sampled by up to six special k points for atomic structure relaxation and a total of 50 k points for electronic-structure calculation. The external electric field is introduced by planar dipole layer method as implemented in VASP.[31]

A schematic illustration of the model geometry used in our calculations is given in Fig. 1. The unit cell of each ZS-GNR consists of wider and narrower sections that are alternatively aligned along the ribbon edge. The length and width of the relatively wide segment are denoted by N_{a1} and N_{z1} (correspondingly, the protruded step length can be denoted by N_{a1}), while those of relatively narrow section are denoted by N_{a2} and N_{z2}, where N_{zi} (i=1 and 2) is the number of zigzag chains across the ribbon width, and N_{ai} (i=1 and 2) is the number of hexagon rings in each section along the ribbon edge. The system is constructed by periodically repeating the above unit cell along the ribbon edge. Consequently, periodic protruded edges are formed in ZS-GNRs. As a result, we can denote the ribbon with protruded edge steps as ZS-GNR(N_{z1}, N_{a1}; N_{z2}, N_{a2}), and the structure of ZS-GNR(12, 4; 6, 4) is illustrated in Fig. 1, for example. The height of the edge step thus can be defined as the $\Delta N_z=(N_{z1}-N_{z2})/2$. To eliminate the effect of the σ electronic states near the Fermi level, we terminate all the dangling bonds at the ribbon edges by hydrogen atoms.

III. RESULTS AND DISCUSSIONS

A. Electronic and magnetic properties of the ZS-GNRs

We take the ZS-GNR(8, N_{a1}; 6, N_{a2}) as a prototype for discussions and explore the variation in properties of the ZS-GNR as a function of N_{a1} and N_{a2}. We first consider the electronic and magnetic properties of smoothly edged ZGNR with eight zigzag chains across the ribbon width. We find that the smooth Z_8-GNR has a direct band gap of 0.30 eV as well as a magnetic insulating ground state with antiferromagnetic coupling between two edges of ferromagnetically ordered edge states. This gap value and character of magnetic ordering are well consistent with previous DFT results.[16] Based on the magnetic ordering in the perfect Z-GNR, we consider the following magnetic phases for the ZS-GNRs: (i) ferromagnetically ordered spins at each ribbon edge and the same spin directions between two edges, denoted by FM; (ii) ferromagnetically ordered spins at each edge but the opposite spin directions between the edges, denoted by AFM; and (iii) nonmagnetic state, denoted by NM. We perform total-energy calculations for the ZS-GNRs with the above-mentioned three magnetic phases. To concisely show the picture, we fix the step height to $\Delta N_z=1$ and consider the ZS-GNR(8, N_{a1}; 6, 2) and ZS-GNR(8, 3; 6, N_{a2}). Then we study the energy relations as a function of the N_{a1} and N_{a2}, respectively. The relative energies of FM, AFM, and NM states for the ZS-GNR(8, N_{a1}; 6, 2) and ZS-GNR(8, 3; 6, N_{a2}) are shown in Table I. It is found that the total-energy difference between the FM and NM phases rapidly increases with the increasing of N_{a1} or N_{a2} for both the ZS-GNRs. An important result from this energy analysis is that both the ZS-GNRs become nonmagnetic when N_{a1} and N_{a2} are less than 4 and 3, respectively, as corroborated by the zero energy difference between the FM and NM phases, although the edge carbons still possess zigzag-shaped edges. On the other hand, when the ZS-GNRs are magnetic, we find that the energy of AFM state is lower than that of the FM state regardless of ribbon geometry, suggesting that AFM are always the ground state and the character of magnetic ordering is akin to that of the smoothly edged ZGNR, although the energy difference between AFM and FM states displays a little oscillation with the increasing of N_{a1} or N_{a2}. To further verify these results, we also performed the same calculations for the magnetic stability of the ZS-GNRs using the GGA approximation with the PW91 functionals. We find the results well consistent with those from LSDA calculations. We then plot the isosurfaces of the magnetization density $(\rho_\uparrow-\rho_\downarrow)$ for the ground state of the ZS-GNR(8, 3; 6, 6) in Fig. 2(a). It is shown that magnetization density is mainly localized at the edges of the nanoribbon and the edge spins are antiferromagnetically

TABLE I. Relative total energies of FM, AFM, and NM states of a ZS-GNR(8, N_{a1}; 6, N_{a2}), which is abbreviated as (N_{a1}; N_{a2}) for simplicity here.

(N_{a1}; N_{a2}) (meV)	(3; 1)	(3; 2)	(3; 3)	(3; 4)	(3; 5)	(3; 6)	(1; 2)	(2; 2)	(4; 2)	(5; 2)	(6; 2)	Z_8-GNR
$N_{NM}-N_{FM}$	0	0	2	9	41	91	0	0	7	26	75	31
$N_{NM}-N_{AFM}$	0	0	13	30	71	107	0	0	16	58	90	34

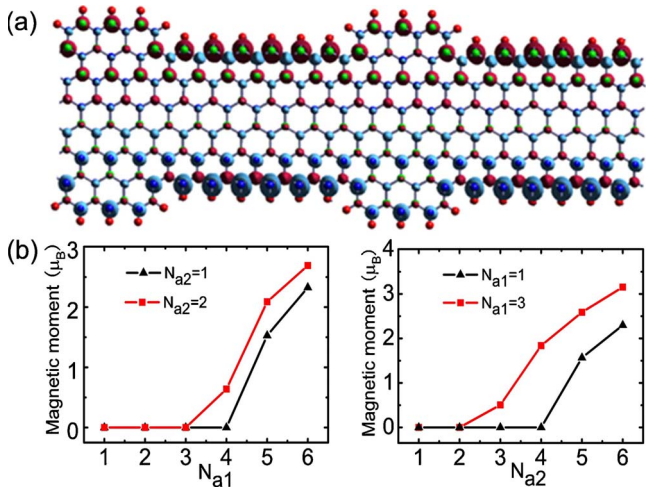

FIG. 2. (Color online) (a) Isosurface plot of the spin-density magnetization ($\rho_\uparrow - \rho_\downarrow$) for the AFM phases of ZS-GNR(8, 3; 6, 6). The red and light blue surfaces represent spin-up and spin-down density, respectively. (b) Variation in half-net magnetic moment as a function of the width of different N_{a1} and N_{a2} for the ZS-GNR(8, N_{a1}; 6, N_{a2}).

coupled with each other. However, there are some differences in the magnetization magnitudes of carbon atom from those in the smoothly edged ZGNRs. It is shown that the local moments are slightly suppressed near the step junction of the structure and the magnetic moments increase gradually when moving away from the step junction. Moreover, the edge magnetization magnitudes are larger in the narrow section, which is longer than the wide section in the direction along the ribbon edge.

We next specially examine the variation in edge magnetization with the structural parameters in the ZS-GNRs. Figure 2(b) plots the half-net magnetic moment per supercell for the ZS-GNR(8, N_{a1}; 6, N_{a2}) as a function of N_{a1} and N_{a2}. Here the half-net magnetic moment is defined as the sum of the local magnetic moments on atoms from the terminated H atoms at one edge to the carbon atoms at the center of the ribbon. For the ZS-GNR(8, 1; 6, N_{a2}), one can see that the spin is completely suppressed when N_{a2} is less than 4, beyond which the half-net magnetic moment gradually increases with the increasing of N_{a2}. We call N_{a2}=4 the critical value for the appearance of spins in ZS-GNRs. We find that the critical N_{a2} decreases with increasing step length, N_{a1}, of the ZS-GNR(8, N_{a1}; 6, N_{a2}). For example, the critical N_{a2} is reduced to 2 for the ZS-GNR(8, 3; 6, N_{a2}). These results indicate that edge magnetization can be efficiently modulated by the protruded edge configuration.

We next explore the underlying mechanism governing the strong dependence of edge magnetization on the edge configuration in the ZS-GNRs. As is well known, the magnetization of pristine Z-GNRs is originated from the exchange splitting of the peculiar edge states which show localization of the electron states as well as a sharp density of states (DOS) peak around the Fermi level.[32] We therefore investigate the change in peaks in the spin-unpolarized DOS at the Fermi level of the ZS-GNRs with different edge configuration. Figure 3 shows the DOS of the ZS-GNR(8, 3; 6, N_{a2}) as

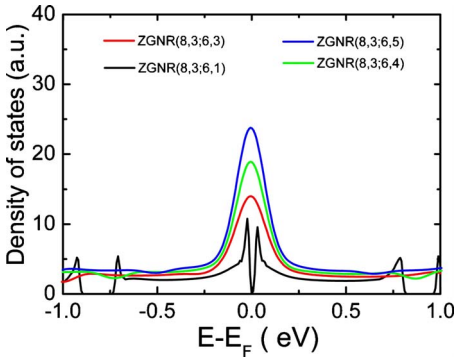

FIG. 3. (Color online) Calculated total spin-unpolarized DOS of ZS-GNR(8, 3; 6, N_{a2}) with N_{a2}=1,3,4,5.

N_{a2} varies from 1 to 5. The DOS at E_F is zero at N_{a2}=1. The zero electronic states at E_F cannot result in instability toward spin splitting and the system is thus in a NM state. With increasing N_{a2}, a DOS peak appears at the Fermi level and gradually increases with the increasing of N_{a2}. We find that the localized DOS is mainly contributed by the edge atoms in the relatively narrow section, indicating that the localized edge states are recovered and enhanced with increasing length of the narrow section. As a result of the sharp DOS peak, strong local electron-electron interaction leads to split of the edge states and formation of edge magnetization. In particular, the DOS magnitude increases with increasing N_{a2} and thereby induces larger spin splitting according to the Stoner criterion. Kumazaki *et al.*[24] have studied the magnetism of similar ribbon structures using the Hubbard model and the results coincide well with our findings.

The above analyses indicate that the magnetic properties of the ZS-GNRs strongly depend on the localized electronic states around the Fermi level. To probe the underline mechanism of why the localized electronic states appear or disappear at the Fermi level, we perform further examination on the spin-unpolarized band structures of involved structures. Figure 4(a) presents the band structure of the ZS-GNR(8, 3; 6, 1), which is a NM semiconductor with a energy gap of 0.04 eV. This nonmagnetic ground state can be understood from the charge densities corresponding to the lowest conduction band and the highest valence band, as shown in the right panel of Fig. 4(a), where we can clearly find some wave nodes, suggesting that the quantum confinement effect is the root of the nonmagnetic ground state and the gap opening. The confinement effect increases the dispersion of the lowest conduction band and the highest valence band and thereby quenches the magnetism, attributed to the short length of the relatively wide and narrow sections alternatively aligned along the ribbon edge. In contrast, when N_{a2} is increased to 2, we find the charge densities for the lowest conduction band and the highest valence band mostly localized at the ribbon edge and the wave nodes become less pronounced. Consequently, the dispersion of the lowest conduction band and the highest valence band decreases, and the gap is closed but the system is still nonmagnetic due to the small DOS at the Fermi level, see Fig. 4(b). With further increasing N_{a2} to 4, the lowest conduction band and the highest valence band become flat and degenerated around the

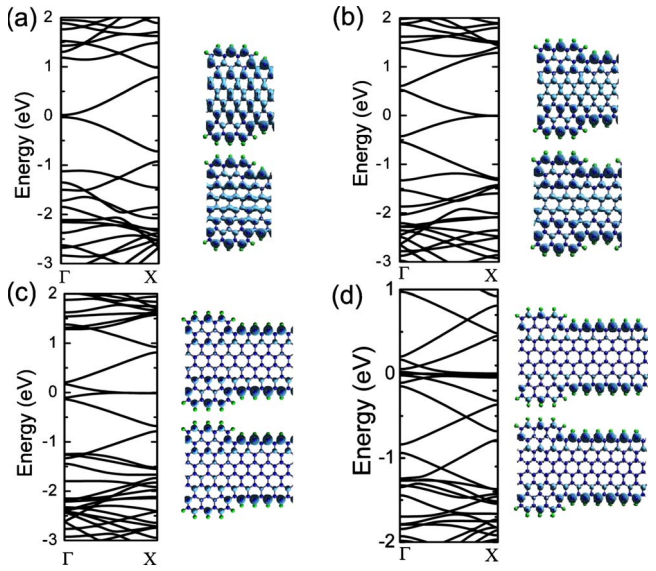

FIG. 4. (Color online) Spin-unpolarized band structures of ZS-GNR(8, 3; 6, N_{a2}) and charge densities corresponding to the lowest conduction band and the highest valence band. The cases for the ZS-GNR(8, 3; 6, 1), (8, 3; 6, 2), (8, 3; 6, 4), and (8, 3; 6, 6) are shown in (a), (b), (c), and (d), respectively.

Fermi level at the wave number close to the center of the Brillouin zone, leading to electronic localization and emerged edge magnetization, see Fig. 4(c). Further increasing N_{a2} will enhance the localization effect of electronic states due to the reduced quantum confinement effect within the relatively narrow ribbon section, as evidenced in Fig. 4(d) for N_{a2}=6. Increasing step length, N_{a1}, will further attenuate the quantum effect imposed on the edge states, thereby giving rise to a magnetic ZS-GNR at smaller N_{a2}.

In addition to the significant magnetic properties, we find that the electronic properties of ZS-GNRs also exhibit interesting change compared to the smoothly edged Z-GNRs. We mainly discuss the influence of edge configuration on the energy gap of ZS-GNRs by changing their N_{a1} and N_{a2}. The band gap of the ZS-GNR(8, 1; 6, N_{a2}) is shown in Fig. 5(a)

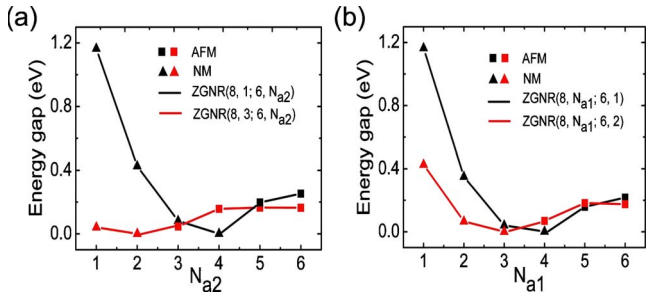

FIG. 5. (Color online) Variation in calculated energy gap of ZS-GNR(8, N_{a1}; 6, N_{a2}) as a function of N_{a1}, N_{a2}. The lines with square represent the system with a AFM ground state while the lines with triangle represents case of systems with a NM ground state.

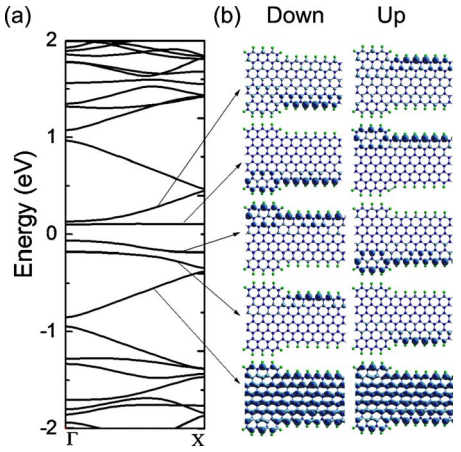

FIG. 6. (Color online) Spin-polarized electronic properties of ZS-GNR(8, 3; 6, 6). (a) Spin-polarized band structure for the AFM ground state. The bands for the up-spin and down-spin states are degenerate. (b) Charge densities of selected specific states.

as a function of N_{a2}, where the band gap decreases first to a minimum at N_{a2}=4 and then increases with increasing N_{a2}. On the left side of the gap minimum, namely, $N_{a2}<4$, the system is nonmagnetic while on the right side the system becomes a magnetic semiconductor with AFM phase. For the nonmagnetic ZS-GNR, the gap is due to the aforementioned quantum confinement effect along the ribbon edges, and is widened to 1.164 eV when N_{a2} decreases to 1, significantly higher than 0.30 eV of the Z_8-GNR with smooth edges. Therefore, the ZS-GNR(8, 1; 6, 1) holds great promise for realizing room-temperature field-effect devices. In fact, recent experiments have demonstrated field-effect devices at room temperature based on Z-GNRs and the edge roughness are probably the underlying condition leading to the behavior. On the other hand, for the magnetic ZS-GNR, the gap is due to the spin splitting of the localized edge states. This spitting is enhanced with increasing the localization of electronic states. However, the gap of the magnetic ZS-GNRs is always smaller than 0.30 eV of the perfect Z_8-GNR due to the insertion of the protruded steps in the ribbon edges that break the electronic localization. Similarly, once N_{a2} is fixed to 1, remarkable gap variation is also observed in the ZS-GNR(8, N_{a1}; 6, 1) when N_{a1} varies from 1 to 6, as shown in Fig. 5(b), and the gap minimum occurs at N_{a1}=4. However, when the fixed N_{a1} is increased to 3, the gap variation in the ZS-GNR(8, 3; 6, N_{a2}) with N_{a2} is largely smoothed compared to that of the ZS-GNR(8, 1; 6, N_{a2}), especially for the nonmagnetic ZS-GNR on the left side of the gap minimum at N_{a2}=2. This is because the quantum confinement effect is attenuated by increasing length of the wide sections. On the right side of the gap minimum, the gap remains basically unchanged. We take ZS-GNR(8, 3; 6, 6) as an example to elucidate the detailed electronic structure; and the spin-polarized band structure as well as the projected charge density isosurface plots for selected specific states are plotted in Fig. 6. Similar to ZS-GNR(8, 1; 6, N_{a2}) ($N_{a2}>4$), the states of opposite spin orientation are degenerate in all bands, and a band gap of 0.16 eV is observed around the Fermi level. Charge-density analyses show that the highest

valence band is distributed around the upper edge while the lowest conduction band is located mainly on the opposite down edge of ZS-GNR(8, 3; 6, 6) for the spin-down state; for the spin-up state the case is just reversed. In contrast, the states associated with the second lowest conduction band and second highest valence band are confined mainly on the narrow segment of ZS-GNR(8, 3; 6, 6) and a rapid decay for these states from the ribbon edge to the interior is also observed.

Actually, the ZS-GNR can be viewed as a infinite thin slab with periodic protruded steps at both the edges. The protruded steps give rise to potential barriers between the wide and narrow segments of the ZS-GNR, which is absent in pure Z-GNRs. When electrons axially transmit through the ZS-GNR, they tend to be confined by the potential barriers. Some of the confined electronic states can just be evidenced in Fig. 6(b). To be more specified, the confinement in the segment N_{ai} can be defined as the integral of the planarly averaged charge, namely, $\int_{N_{ai}}|\Psi(\mathbf{r})|^2 d\mathbf{r}$. From this definition, it is obvious that the confinement of electronic states would become stronger with the increasing of $\Delta N_z=(N_{z1}-N_{z2})/2$. For ZS-GNRs with smaller N_{ai}, the electronic states would be more distinguished from those of smoothly edged ZGNR. On the other hand, increasing the N_{a1} or N_{a2} will make the electronic properties in the corresponding segment gradually close to those of smoothly edged ZGNRs.

Based on these results, we infer that the ZS-GNR would always own an AFM phase if the length of either the wide or the narrow sections becomes sufficiently long. Indeed, our extensive calculations show that when N_{a1} is larger than 4, namely, a step length of 9.776 Å, the ZS-GNR(8, N_{a1}; 6, N_{a2}) is AFM semiconductor irrespective of N_{a2}. We also discuss briefly the influence of the height of the edge step (ΔN_z) on the electronic and magnetic properties of ZS-GNRs. We increase ΔN_z from 1 used in the above discussion to 3. It is found that all the trend of gap variation with the edge configuration remains essentially the same. For example, with increasing N_{a1} in the ZS-GNR(12, N_{a1}; 6, 2) ($\Delta N_z=3$), the system is NM semiconductor at $N_{a1}=2$ with a direct gap of 0.05 eV, then switched to be NM metal at $N_{a1}=3$, and finally becomes a magnetic semiconductor when $N_{a1}>3$. The trend is exactly the same as that of the ZS-GNR(8, N_{a1}; 6, 2) ($\Delta N_z=1$). Nevertheless, the energy gap can be slightly reduced by increasing height of the step. The direct band gap is 0.07 eV for the ZS-GNR(8, 2; 6, 2) with $\Delta N_z=1$ but is reduced to 0.05 eV for the ZS-GNR(12, 2; 6, 2) with $\Delta N_z=3$ and to 0.03 eV for ZS-GNR(20, 2; 6, 2) with $\Delta N_z=7$. Moreover, the confined states can occur in wide segment of the ZS-GNR(N_{z1}, N_{a1}; N_{z2}, N_{a2}) when N_{z1} and N_{z2} increase.

B. Energy-gap modulation of the ZS-GNRs by transverse electric field

The external electric field has been demonstrated to be capable of efficiently modulating the electronic and magnetic properties of many carbon nanostructures. In particular, half metallicity is predicted in smoothly edged Z-GNRs when an external transverse electric field is applied.[17] Therefore, it should be interesting to investigate the corresponding response of the ZS-GNRs to applied transverse electric fields (E_{ext}).

In the study of field-induced modulation of electronic properties, the ZS-GNR(8, 3; 6, 1), ZS-GNR(8, 3; 6, 2), and ZS-GNR(8, 3; 6, 4) are chosen to represent the three typical families, corresponding to the NM semiconductor, NM metal, and AFM semiconductor, respectively. The electric field is applied across the zigzag-shaped edges of the ZS-GNRs, as illustrated in Fig. 7(a). Figures 7(b) and 7(c) show the response of energy gap to E_{ext} for the first two NM ZS-GNRs. For the metallic ZS-GNR(8, 3; 6, 2), surprisingly, we find that the band gap opens up and enhances linearly with increasing E_{ext}, rendering a field-induced metal insulator in the ZS-GNR at an extremely small field strength. The band structure of ZS-GNR(8, 3; 6, 2) at 0.4 V/Å is shown in Fig. 7(e). Compared to the band structure without the external electric field shown in Fig. 4(b), the band degeneracy are broken owing to the applied E_{ext}. The charge densities for the lowest conduction band and the highest valence band are plotted in Fig. 7(f). When E_{ext} is applied, the lowest conduction band is located mainly on the lower edge of ZS-GNR(8, 3; 6, 2), while the highest valence band is located on the upper edge. All the distributions of charge density are remarkably different from those without an external electric field shown in Fig. 4(b). Thereby, the band gap opening can be ascribed to the Stark effect, which has been observed in previous studies on carbon nanotubes[33] and boron nitride (BN) ribbons.[34] For the NM semiconducting ZS-GNR(8, 3; 6, 1), the response of energy gap to E_{ext} is similar to that of above-mentioned metallic ZS-GNR(8, 3; 6, 2). The gap gradually increases with the increasing of E_{ext} and can be 0.22 eV when E_{ext} is up to 0.5 V/Å. Such field-induced engineering of band gap highlights an innovative route for GNR-based nanoelectronic and nanophotonic devices.

To have a deeper insight into the field-induced gap modification for the metallic and semiconducting ZS-GNRs, we further analyze the system symmetry. As is well known, there exists mirror reflection symmetry in the smoothly edged Z_8-GNR, offering a single mirror-symmetry plane σ. The peculiar doubly degenerate flat edge states mix to form bonding and antibonding states (i.e., π and π^* subbands) (Ref. 35) when spins are not considered. The two eigenstates are degenerated and present a well-defined parity with respect to this symmetry plane. The wave functions of $\pi^*(\pi)$ subbands have even (odd) parities under σ mirror operation. Due to the protruded edge steps, the mirror symmetry of the system becomes lower. However, the ZS-GNR studied in our calculations retains a single mirror-symmetry plane in absence of an external electric field. When an external electric field is applied as shown in Fig. 7(a), the mirror symmetry is broken, resulting in the π and π^* states having no definite σ parity. The π and π^* states will couple with each other and become hybridized. Therefore, the degeneracy is lifted and the band gap opens up rapidly with increasing E_{ext}, as shown in Figs. 7(b) and 7(c).

For the ZS-GNRs with the AFM ground state, we find that the gap change is spin dependent and half metallicity is realized by the applied electric field. The energy gaps for both

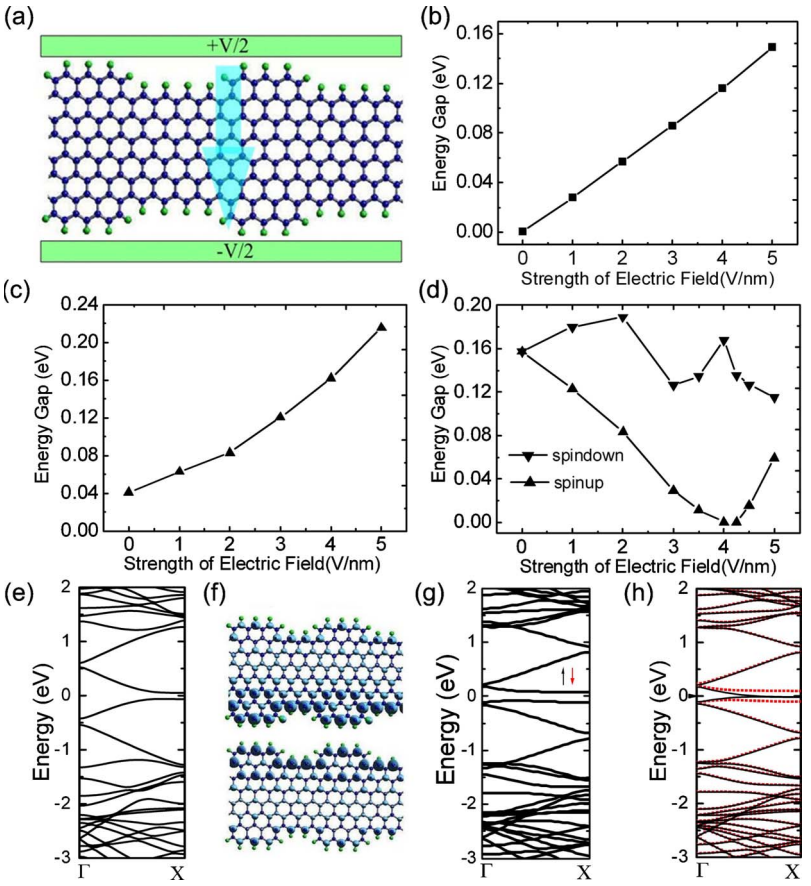

FIG. 7. (Color online) Electronic properties of ZS-GNRs with external transverse electric fields. (a) Diagram of ZS-GNRs with the electric fields. The positive direction of E_{ext} is denoted by a big arrow and the infinitely extended direction is perpendicular to that of E_{ext}. (b)–(d) plot the energy gap modification of ZS-GNR(8, 3; 6, 2), (8, 3; 6, 1), and (8, 3; 6, 4) as a function of E_{ext}, respectively. (e) The band structure of ZS-GNR(8, 3; 6, 2) at E_{ext}=0.4 V/Å. The system has no spin polarization. (f) Charge densities for the lowest conduction band and the highest valence band of the ZS-GNR(8, 3; 6, 2) at E_{ext}=0.4 V/Å. [(g) and (h)] Spin-polarized band structure of ZS-GNR(8, 3; 6, 4) at fields of (g) 0.0 and (h) 0.4 V/Å.

spin states of ZS-GNR(8, 3; 6, 4) are plotted as a function of applied field strength in Fig. 7(d). When $E_{ext} \leq 0.2$ V/Å, the gap for up spin decreases while that for the down spin increases as E_{ext} increases. Because oppositely oriented spin states are located at the opposite sides of the ZS-GNR, the electric field has an opposite effect on the two spin states. This makes the occupied spin-up states upshift and the unoccupied spin-up states downshift as E_{ext} increases, thereby narrowing the energy gap for the spin-up state. On the contrary, the occupied and unoccupied spin-down states move apart with each other to enlarge the energy gap. These are similar to the smoothly edged Z-GNRs.[17] When $E_{ext} > 0.2$ V/Å, the energy gap of spin-up state continues to decrease as E_{ext} increases and becomes zero when E_{ext} reaches 0.4 V/Å. Nevertheless, significant difference occurs for the spin-down state as shown by Fig. 7(d). The occupied and unoccupied spin-down states display a fluctuation behavior in energy with a oscillation around 0.1574 eV, which corresponds to the gap of ZS-GNR(8, 3; 6, 4) without applied field. The fluctuation behavior of the energy gap for the spin-down state is not observed in smoothly edged Z-GNRs. The critical electric field for achieving half metallicity in the ZS-GNR(8, 3; 6, 4) is around 0.4 V/Å. The corresponding band structure for the ZS-GNR(8, 3; 6, 4) under 0.4 V/Å is shown in Fig. 7(h), where a half metal is clearly featured around the Fermi level. Therefore, a perfect spin filter can be designed based on such kinds of ribbons using lower electric field.

IV. CONCLUSION

In summary, extensive density-functional theory calculations reveal that ZS-GNRs have novel electronic and magnetic properties depending strongly on the protruded edge step structures. With the protruded step less than 9.776 Å, the system can be converted from a nonmagnetic semiconductor to metal and then to a magnetic semiconductor with the magnetic ordering similar to that of a smoothly edged Z-GNRs, as the step-to-step distance continuously increases. The half-net magnetic moment and energy gap can be effectively modulated by changing the edge configuration of the ZS-GNRs. However, with the protruded step length larger than 9.776 Å, the system will become magnetic semiconducting. In addition, the applied transverse electric field can efficiently modulate the electronic and magnetic properties of the ZS-GNRs, especially inducing metal-insulator transition and continuously tunable band gap in the NM ZS-GNRs as well as a half metallicity for the magnetic ZS-GNRs. Our systematic study of the electronic and magnetic properties indicates that ZS-GNRs are promising for future nanoelectronics and spintronics and could even be superior to the smoothly edged GNRs for applications in some fields.

ACKNOWLEDGMENTS

This work is supported by the 973 Program (Grant No. 2007CB936204), National NSF (Grant No. 10732040), and Jiangsu Province NSF (Grant No. BK2008042).

*wlguo@nuaa.edu.cn

[1] K. S. Novoselov, A. K. Geim, S. V. Morozov, D. Jiang, M. I. Katsnelson, I. V. Grigorieva, S. V. Dubonos, and A. A. Firsov, Nature (London) **438**, 197 (2005).

[2] Y. Zhang, Y. Tan, H. L. Stormer, and P. Kim, Nature (London) **438**, 201 (2005).

[3] K. S. Novoselov, D. Jiang, F. Schedin, T. J. Booth, V. V. Khotkevich, S. V. Morozov, and A. K. Geim, Proc. Natl. Acad. Sci. U.S.A. **102**, 10451 (2005).

[4] J. Tworzydło, B. Trauzettel, M. Titov, A. Rycerz, and C. W. J. Beenakker, Phys. Rev. Lett. **96**, 246802 (2006).

[5] S. V. Morozov, K. S. Novoselov, M. I. Katsnelson, F. Schedin, L. A. Ponomarenko, D. Jiang, and A. K. Geim, Phys. Rev. Lett. **97**, 016801 (2006).

[6] A. F. Morpurgo and F. Guinea, Phys. Rev. Lett. **97**, 196804 (2006).

[7] K. S. Novoselov, E. McCann, S. V. Morozov, V. I. Fal'ko, M. I. Katsnelson, U. Zeitler, D. Jiang, F. Schedin, and A. K. Ceim, Nat. Phys. **2**, 177 (2006).

[8] D. Gunlycke, D. A. Areshkin, J. Li, J. W. Mintmire, and C. T. White, Nano Lett. **7**, 3608 (2007).

[9] H. B. Heersche, P. Jarillo-Herrero, J. B. Oostinga, L. M. K. Vandersypen, and A. F. Morpurgo, Nature (London) **446**, 56 (2007).

[10] Y. Guo, W. Guo, and C. Chen, Appl. Phys. Lett. **92**, 243101 (2008).

[11] K. S. Novoselov, A. K. Geim, S. V. Morozov, D. Jiang, Y. Zhang, S. V. Dubonos, I. V. Grigorieva, and A. A. Firsov, Science **306**, 666 (2004).

[12] F. Schedin, A. K. Geim, S. V. Morozov, E. W. Hill, P. Blake, M. I. Katsnelson, and K. S. Novoselov, Nat. Mater. **6**, 652 (2007).

[13] W. Y. Kim and K. S. Kim, Nat. Nanotechnol. **3**, 408 (2008).

[14] C. Berger, Z. M. Song, X. B. Li, X. S. Wu, N. Brown, C. Naud, D. Mayo, T. B. Li, J. Hass, A. N. Marchenkov, E. H. Conrad, P. N. First, and W. A. de Heer, Science **312**, 1191 (2006).

[15] X. Li, X. Wang, L. Zhang, S. Lee, and H. Dai, Science **319**, 1229 (2008).

[16] Y. W. Son, M. L. Cohen, and S. G. Louie, Phys. Rev. Lett. **97**, 216803 (2006).

[17] Y. W. Son, M. L. Cohen, and S. G. Louie, Nature (London) **444**, 347 (2006).

[18] Z. Zhang, C. Chen, and W. Guo, Phys. Rev. Lett. **103**, 187204 (2009).

[19] A. L. Elías, A. R. Botello-Méndez, D. Meneses-Rodríguez, V. J. González, D. Ramirez-González, L. Ci, E. Muñoz-Sandoval, P. M. Ajayan, H. Terrones, and M. Terrones, Nano Lett. **10**, 366 (2010).

[20] B. Huang, F. Liu, J. Wu, B. L. Gu, and W. H. Duan, Phys. Rev. B **77**, 153411 (2008).

[21] P. Koskinen, S. Malola, and H. Häkkinen, Phys. Rev. Lett. **101**, 115502 (2008).

[22] T. B. Martins, A. J. R. da Silva, R. H. Miwa, and A. Fazzio, Nano Lett. **8**, 2293 (2008).

[23] O. V. Yazyev and M. I. Katsnelson, Phys. Rev. Lett. **100**, 047209 (2008).

[24] H. Kumazaki and D. S. Hirashima, J. Phys. Soc. Jpn. **77**, 044705 (2008).

[25] B. Huang, M. Liu, N. Su, J. Wu, W. Duan, B. L. Gu, and F. Liu, Phys. Rev. Lett. **102**, 166404 (2009).

[26] Z. Zhang and W. Guo, Appl. Phys. Lett. **95**, 023107 (2009).

[27] E. Kan, Z. Li, J. Yang, and J. G. Hou, J. Am. Chem. Soc. **130**, 4224 (2008).

[28] Z. Wu, J. B. Neaton, and J. C. Grossman, Phys. Rev. Lett. **100**, 246804 (2008).

[29] G. Kresse and J. Furthmüller, Phys. Rev. B **54**, 11169 (1996).

[30] D. Vanderbilt, Phys. Rev. B **41**, 7892 (1990).

[31] J. Neugebauer and M. Scheffler, Phys. Rev. B **46**, 16067 (1992).

[32] M. Fujita, K. Wakabayashi, K. Nakada, and K. Kusakabe, J. Phys. Soc. Jpn. **65**, 1920 (1996).

[33] J. O'Keeffe, C. Y. Wei, and K. J. Cho, Appl. Phys. Lett. **80**, 676 (2002).

[34] Z. Zhang and W. Guo, Phys. Rev. B **77**, 075403 (2008).

[35] T. B. Martins, R. H. Miwa, A. J. R. da Silva, and A. Fazzio, Phys. Rev. Lett. **98**, 196803 (2007).